Climate Dynamics manuscript No.
(will be inserted by the editor)

Impact of Improved Representation of Horizontal and Vertical Cloud Structure in a Climate Model

Jonathan K. P. Shonk · **Robin J. Hogan** · **James Manners**

Received: date / Accepted: date

Abstract Many studies have investigated the effects that misrepresentation of sub-grid cloud structure can have on the radiation budget. In this study, we perform twenty-year simulations of the current climate using an atmosphere-only version of the Met Office Unified Model to investigate the effects of cloud approximation on model climate. We apply the "Tripleclouds" scheme for representing horizontal cloud inhomogeneity and "exponential-random" overlap, both separately and in combination, in place of a traditional plane-parallel representation with maximum-random overlap, to the clouds within the radiation scheme. The resulting changes to both the radiation budget and other meteorological variables, averaged over the twenty years, are compared. The combined global effect of the parameterizations on top-of-atmosphere short-wave and long-wave radiation budget is less than 1 W m^{-2}, but changes of up to 10 W m^{-2} are identified in marine stratocumulus regions. A cooling near the surface over the winter polar regions of up to 3°C is also identified when horizontal cloud inhomogeneity is represented, and a warming of similar magnitude is found when exponential-random overlap is implemented. Corresponding changes of the same sign are also found in zonally averaged temperature, with maximum changes in the upper tropical troposphere of up to 0.5°C. Changes in zonally averaged cloud fraction in this location were of opposite sign and up to 0.02. The individual effects on tropospheric temperature of improving the two components of cloud structure are of similar magnitudes to about 2% of the warming created by a quadrupling of carbon dioxide.

J. K. P. Shonk · R. J. Hogan
Department of Meteorology, University of Reading, Earley Gate, Reading RG6 6BB, Berkshire, UK.
Tel: +44 118 3786979. E-mail: j.k.p.shonk@reading.ac.uk

J. Manners
Met Office, Fitzroy Road, Exeter EX1 3PB, Devon, UK.

Keywords cloud structure; Tripleclouds; exponential-random overlap.

1 Parameterization of Clouds

Clouds present the meteorological community with many great challenges, both in terms of their observation and their representation in weather and climate models. Much uncertainty stems from the complex structure of the cloud and the cloud–radiation feedback processes that control their evolution (Stephens, 2005; Randall et al, 2007). However, modelling clouds with sufficient resolution to capture all of these interactions is far beyond the capability of modern supercomputers. This is particularly true for climate models: their gridboxes are typically 100 km to 200 km in horizontal size.

An issue that needs addressing in terms of cloud modelling is the representation of cloud structure, as changes to many properties of clouds can have significant effects on the interaction of the cloud with radiation (for example, Slingo, 1990). Over the course of a long climate simulation, if these properties are inadequately represented, the outcome of the simulation could be drastically affected. It is well-recognised that the traditional use of plane-parallel (horizontally homogeneous) clouds introduces biases into a model radiation budget. For example, Shonk and Hogan (2008) found top-of-atmosphere cloud radiative forcing to be about 8% too high in magnitude in both the short-wave and long-wave when using plane-parallel clouds. Several studies have dealt with this issue by proposing methods of accounting for horizontal cloud inhomogeneity (for example, Cahalan et al, 1994; Oreopoulos and Barker, 1999; Pomroy and Illingworth, 2000; Carlin et al, 2002; Pincus et al, 2003). One such scheme was introduced by Shonk and Hogan (2008): referred to as "Tripleclouds", it replaces the single value of mean cloud water content in the cloudy part

of a gridbox layer with a two-point distribution, the two values being equally weighted. This process has the effect of dividing the cloud into two equal regions – one containing optically thicker cloud, the other containing optically thinner cloud. For mixed-phase clouds, the ice and liquid particles are assumed to be homogeneously mixed. Both the ice and liquid water contents in the optically thinner region are reduced from their respective mean values by the same fraction, and conversely in the optically thicker region. This results in two regions of different optical depths but the same ice-to-liquid ratio.

Furthermore, it has been more recently noted that the traditional maximum-random cloud overlap scheme of Geleyn and Hollingsworth (1979) could also be a source of bias in the radiation budget (Barker et al, 1999). In response, a new scheme for representing vertical cloud alignment, referred to as "exponential-random" overlap, was introduced by Hogan and Illingworth (2000). They defined an "overlap parameter", which allows the combined cloud cover of a pair of gridbox layers to take any value between that of maximum overlap and of random overlap. They found overlap parameter to decay exponentially with separation for pairs of layers within a block of vertically continuous cloud. The global distribution of the corresponding vertical decorrelation scale was investigated by Barker (2008), and a latitude-dependent parameterization of it was created by Shonk et al (2010), describing overlap between pairs of adjacent layers.

Shonk and Hogan (2010) applied Tripleclouds and exponential-random overlap, both separately and in combination, to a sample of scenes from a year of re-analysis data from the European Centre for Medium-Range Weather Forecasts (ECMWF). They investigated the impacts of the two parameterizations on the global radiation budget in terms of top-of-atmosphere cloud radiative forcing (CRF; the change in net downward radiative flux that is due to the presence of clouds). They found the inclusion of horizontal inhomogeneity by Tripleclouds to reduce the magnitude of top-of-atmosphere net CRF by 4.13 W m^{-2} and the improvement of vertical overlap representation by exponential-random to enhance it by 1.88 W m^{-2}. These correspond to percentage changes of 12.6% and 5.7% with respect to the CRF calculated for plane-parallel clouds aligned with maximum-random overlap. The combined effect of the two components was a decrease of 2.25 W m^{-2} (6.9%), but with much larger effects of more than 10 W m^{-2} in regions of marine stratocumulus.

The question then arises as to what effect the same parameterizations will have in a free-running climate model, where the changes to the radiation budget are allowed to influence the cloud distribution and atmospheric temperature structure. In this study, we attempt to answer this question by performing the same experiments as Shonk and Hogan (2010), but using the parameterizations in the radiation scheme of the Met Office climate model during a series of climate simulations. We quantify the effects of cloud structure on the radiative budget of the model, and investigate the effects the parameterizations have on other meteorological and dynamical quantities. A fuller description of the method used in this investigation appears in the following section. In section 3, we evaluate the changes in output from the climate model runs and propose possible mechanisms for these changes.

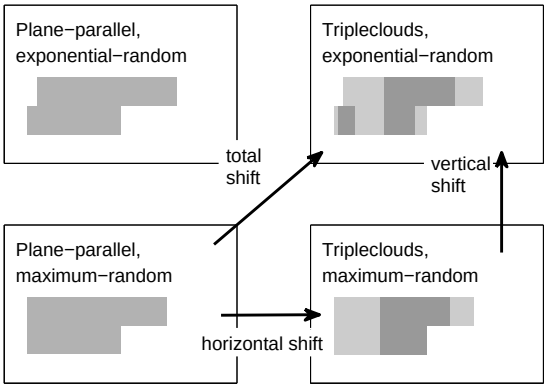

Fig. 1 The cloud representations used in this investigation, and their abbreviations. Each panel shows the alignment of a pair of cloudy layers with cloud fractions of 0.6 and 0.4 in the upper and lower layers respectively for each of the representations. (The plane-parallel, exponential-random configuration is shown here for completeness; it is not used in the experiment.) Changes in an output field that are due to a change of cloud approximation are referred to as "shifts" and are indicated by the arrows.

2 Experimental Setup

The climate model used in this study is an atmosphere-only version of the Met Office Unified Model. We use the Met Office Global Atmosphere Configuration 1.0, with a few modifications: both the Brown and Francis (1995) ice particle densities and the effects of orographic slopes on radiation are included. We also use the modifications to the solver that deal with anomalous horizontal photon transport between regions, described by Shonk and Hogan (2008). Our grid resolution is about 1.80° in longitude and 1.25° in latitude and has 63 vertical levels, most layers being in the troposphere. The native radiation code to the Unified Model is the Edwards–Slingo code (Edwards and Slingo, 1996) and the model timestep is set to give eight radiation calculations per day. Tripleclouds is used to represent horizontal cloud inhomogeneity and exponential-random overlap improves representation of vertical cloud structure. These are applied with the same settings as Shonk and Hogan (2010): fractional standard deviation f_w is fixed to 0.75 globally, and

decorrelation height $Z_{0\beta}$ (in km) is determined from latitude ϕ (in degrees) via:

$$Z_{0\beta} = 2.174 - 0.0207\phi \, .$$

Changes to the cloud representation are only made in the radiation code, so any changes to model output will be via effects on radiation budget. No changes are made to the cloud scheme.

The choice of f_w and $Z_{0\beta}$ by Shonk and Hogan (2010) was based on a review of a number of studies that investigated cloud structure (Shonk et al, 2010). Their value of f_w was determined as the mean fractional standard deviation of water content from some of the studies; their latitude dependence of $Z_{0\beta}$ was a linear fit of overlap decorrelation height scales extracted from other studies. A similar relationship has now been implemented in the ECMWF model (JJ Morcrette, personal communication). Uncertainties in f_w and $Z_{0\beta}$ were also estimated, and the effects of these uncertainties on global radiation budget quantified. They found little sensitivity of radiation budget to $Z_{0\beta}$, with its uncertainty varying global mean net CRF by less than 0.5 W m^{-2}. A more marked sensitivity to f_w was found: varying f_w in the range 0.75 ± 0.18 was found to have impacts on radiation budget of order 2 W m^{-2}. However, the effect of this uncertainty on model simulations is beyond the scope of this study.

We use the same approach to quantify the effects of the two parameterizations as in Shonk and Hogan (2010). The control run uses the default plane-parallel clouds with maximum-random overlap (PPm). A second run replaces plane-parallel clouds with horizontally inhomogeneous clouds (represented using the Tripleclouds scheme; TCm); a third run then replaces maximum-random overlap with exponential-random overlap, which improves the representation of vertical cloud overlap (TCe). These cloud representations are shown schematically for a pair of partly cloudy layers in figure 1. Twenty-year runs of the Unified Model are performed for each of the three cloud representations. The runs simulate current climate conditions, running from 1979 to 1998. Greenhouse gases are fixed at constant values typical of current levels; aerosols are allowed to vary and the effects of volcanic eruptions in the period are included. We use an atmosphere-only configuration: both the properties of the sea and of sea ice are prescribed by observed values through this period.

We evaluate the performance of the three runs by comparing the changes in various output fields that are due to the changes in horizontal and vertical cloud structure. These fields are extracted as both annual and seasonal means, but averaged over the full twenty-year period. As in Shonk and Hogan (2010), we describe these changes as "shifts": the horizontal shift is the change in a quantity caused by the introduction of horizontal inhomogeneity; the vertical shift is the change caused by the improvement of vertical overlap. The arrows in figure 1 indicate the pairs of experiments that are compared to calculate a given shift. The choice of the "path" via TCm in preference to the "path" via PPe was made arbitrarily. It should be noted that, as the application of exponential-random overlap differs slightly when a two region, plane-parallel consideration is made, the individual horizontal and vertical shifts on the two paths for a given quantity will be different. By definition, though, the total shifts must be the same irrespective of path.

Table 1 Global mean values of cloud radiative forcing (CRF), and shifts in CRF generated by improvements in representation of cloud horizontal and vertical structure, for this study (top rows) and for Shonk and Hogan (2010; middle rows). Percentages with respect to the CRF calculated for plane-parallel, maximum-random clouds are given. For comparison, we also include the mean CRFs from ERBE (Ramanathan et al, 1989).

	SW CRF / W m^{-2}	LW CRF / W m^{-2}	Net CRF / W m^{-2}
This study (Unified Model)			
Global mean	−36.41	21.79	−14.62
Horizontal shift	3.50	−2.85	0.65
	(−9.6%)	(−13.1%)	(−4.4%)
Vertical shift	−2.38	2.15	−0.23
	(6.5%)	(9.9%)	(1.6%)
Total shift	1.12	−0.70	0.40
	(−3.1%)	(−3.2%)	(−2.7%)
Shonk and Hogan, 2010 (ERA-40 data)			
Global mean	−49.72	16.94	−32.78
Horizontal shift	6.15	−2.02	4.13
	(−12.4%)	(−11.9%)	(−12.6%)
Vertical shift	−3.86	1.98	−1.88
	(7.8%)	(11.7%)	(5.7%)
Total shift	2.29	−0.04	2.25
	(−4.6%)	(−0.2%)	(−6.9%)
Data from ERBE			
Global mean	−48.05	30.98	−17.08

3 Global Effects of Cloud Structure

3.1 Shifts in top-of-atmosphere cloud radiative forcing

We begin by considering the changes in radiation budget. The twenty-year global mean shifts in top-of-atmosphere cloud radiative forcing (CRF) are presented in the top rows of table 1. The global distribution of short-wave and long-wave CRF in the control (PPm) run is shown in figure 2, and the horizontal and vertical shifts are shown in figures 3 and 4. All of the means are extracted from the radiative fields calculated by the model during the course of the runs. It is seen that the horizontal shifts act to decrease the magnitude of the CRF; the vertical shifts act to increase it (short-wave CRF being negative in sign, long-wave CRF being positive in sign, as seen in figure 2). The global mean shifts are of

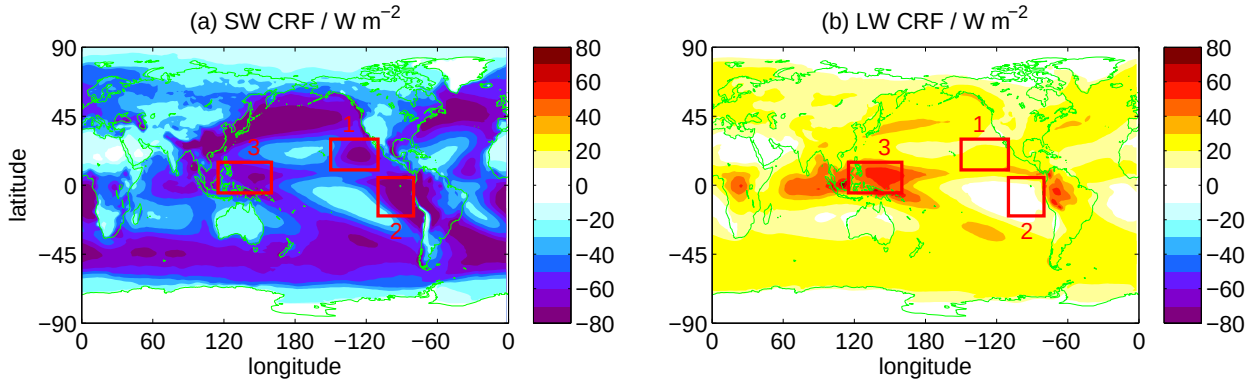

Fig. 2 Global distribution of top-of-atmosphere CRF, calculated for plane-parallel clouds aligned using maximum-random overlap, and averaged over all twenty years of the climate run. The boxes marked on the plot indicate areas of interest referred to in the text: boxes 1 and 2 are areas where marine stratocumulus prevails; box 3 typically contains deep tropical convection.

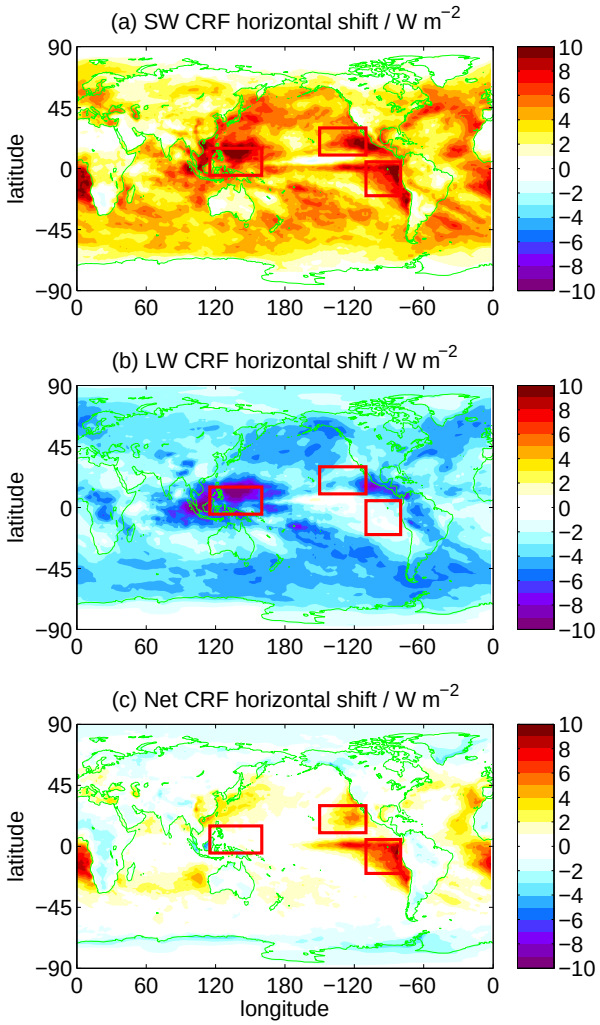

Fig. 3 Global distribution of "horizontal shift" in top-of-atmosphere CRF (the difference in cloud radiative forcing when horizontal inhomogeneity is represented using Tripleclouds as opposed to the plane-parallel approximation; TCm minus PPm). Overlap is represented using maximum-random; (a) short-wave, (b) long-wave and (c) net CRF shifts are shown. The boxes from figure 2 are included.

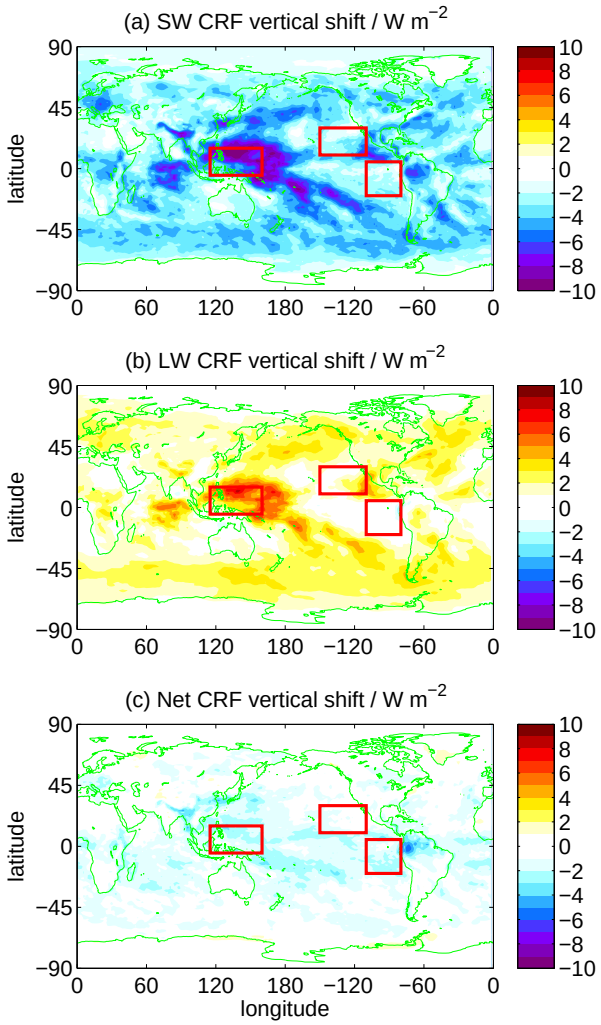

Fig. 4 Global distribution of "vertical shift" in top-of-atmosphere CRF (the difference in cloud radiative forcing when vertical overlap is represented using exponential-random overlap as opposed to maximum-random overlap; TCe minus TCm). Horizontal structure is represented using Tripleclouds; (a) short-wave, (b) long-wave and (c) net CRF shifts are shown. The boxes from figure 2 are included.

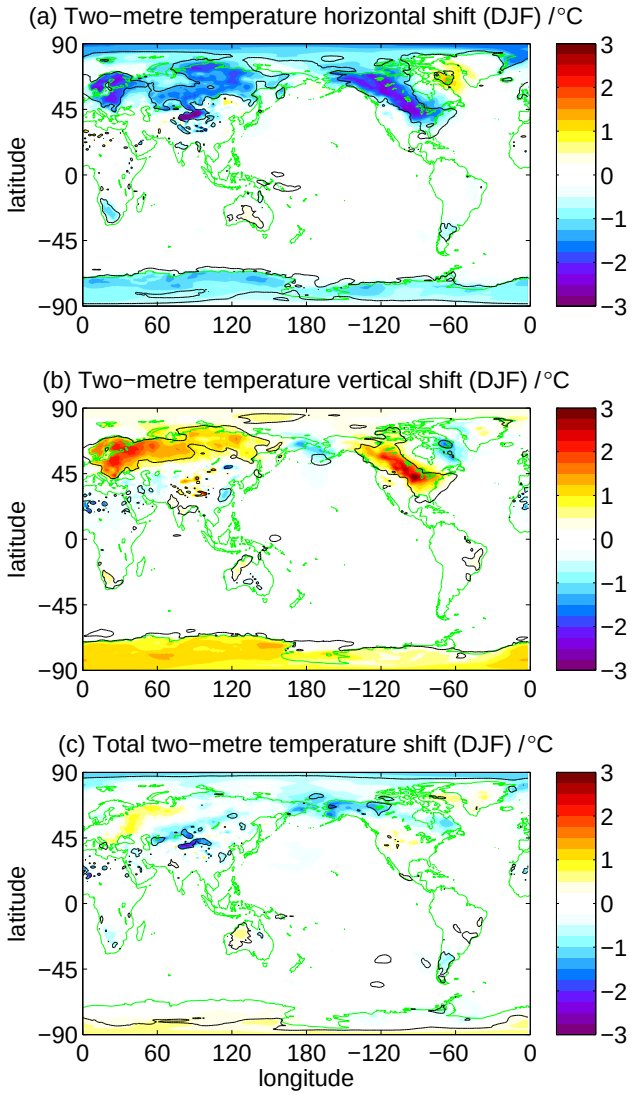

Fig. 5 Global distribution of shifts in two-metre temperature, averaged over December, January and February of each of the twenty years of the climate run: (a) horizontal shift, TCm minus PPm; (b) vertical shift, TCe minus TCm; and (c) total shift, TCe minus PPm. The black contour encloses regions where significance is greater than 95%.

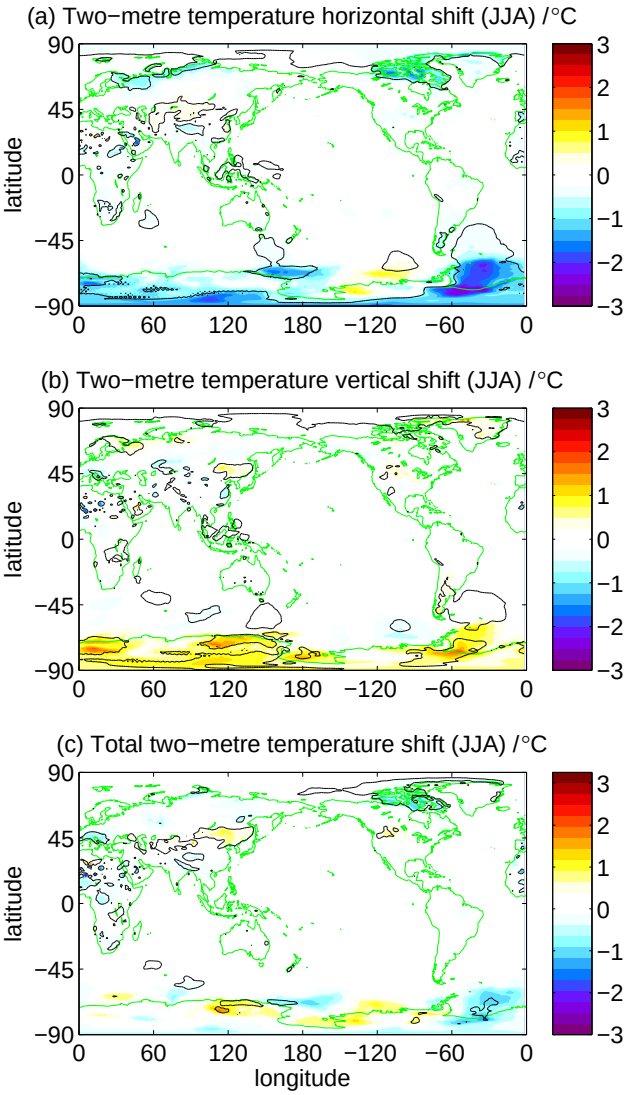

Fig. 6 Global distribution of shifts in two-metre temperature, averaged over June, July and August of each of the twenty years of the climate run: (a) horizontal shift, TCm minus PPm; (b) vertical shift, TCe minus TCm; and (c) total shift, TCe minus PPm. The black contour encloses regions where significance is greater than 95%.

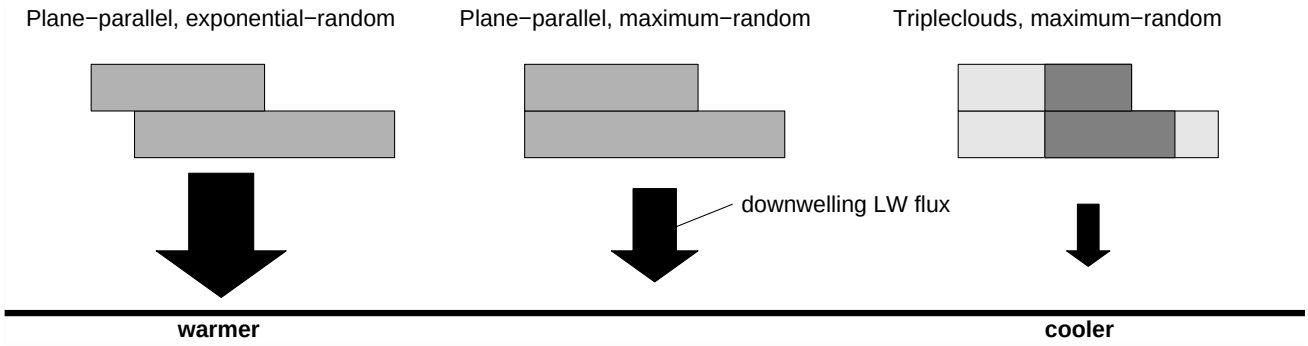

Fig. 7 Schematic showing the radiative processes that drive the two-metre temperature changes over the winter poles. With respect to the plane-parallel, maximum-random case, improving the representation of vertical overlap increases the cloud cover and hence the amount of downward long-wave radiation, causing a local warming; improving the representation of horizontal structure decreases the cloud emissivity and hence the amount of downward long-wave radiation, causing a local cooling.

order 2 to 3 W m^{-2}, but there are some locations where the shifts are much larger.

We identify three important regions of the Pacific, indicated by the red boxes in figures 2, 3 and 4: the areas of marine stratocumulus off the west coast of the major continents (boxes 1 and 2) and the areas of deep tropical convection prevalent over the islands of the western Pacific (box 3). The largest horizontal shifts in net CRF are found in marine stratocumulus. The main effect of introducing cloud inhomogeneity is to reduce both the short-wave albedo and long-wave emissivity of the cloud. Marine stratocumulus covers large areas of ocean and interacts strongly with short-wave radiation, generating a large short-wave CRF. It forms typically in a shallow layer, implying that cloud top temperature is close to the surface temperature, giving a much smaller long-wave CRF. The horizontal shifts in these areas when expressed as a percentage (not shown) turn out to be of comparable size (about 20%) for both the short-wave and the long-wave. This means that the short-wave effect dominates, giving horizontal shifts in net CRF of order 10 W m^{-2}. In the areas of tropical convection, the short-wave CRF is also large, as convection takes place over a wide area. The difference here is that the long-wave CRF is large too, as convective clouds tend to be much deeper, and have much colder cloud-top temperatures. Again, the shifts in percentage terms are about 20% in both the short-wave and long-wave. The absolute horizontal short-wave and long-wave shifts are therefore of comparable size, hence cancel each other out and give a near-zero horizontal shift in net CRF.

The effect of modifying vertical cloud overlap is to change cloud cover, hence larger vertical shifts occur where clouds are tall and partially cover a gridbox. In marine stratocumulus, neither short-wave nor long-wave vertical shifts are evident, as these clouds form in shallow layers and cover vast areas, typically giving cloud covers close to one. In contrast, deep tropical convective clouds span many layers and have cloud fractions much less than one. Hence a small change in overlap assumption can have a much larger effect on cloud cover. These changes give rise to the sizeable shifts in both short-wave and long-wave CRF in these locations. However, as they are of similar size, the vertical shift in net CRF turns out to be near zero.

Table 1 compares the global mean CRF from our twenty-year runs of the Unified Model with those from the ERA-40 scenes evaluated by Shonk and Hogan (2010), along with the horizontal, vertical and total shifts. While the signs of the values presented in the table are all the same, there are some large differences in magnitudes. The global mean net CRF in the ERA-40 data, for example, is seen to be more than twice the magnitude of that in our Unified Model results (-32.78 W m^{-2} in contrast to -14.62 W m^{-2}). If we partition the CRF into short-wave and long-wave, it is revealed that most of the difference originates in the short-wave, and is found to be attributable to differences in global cloud distribution generated by the Unified Model and the ECMWF's Integrated Forecast System (IFS; the model from which the ERA-40 dataset was generated). The principal contributor is the large difference in boundary-layer cloud occurrence: the vertical profile of global-mean cloud fraction exhibits a peak at around 900 hPa in both models, but with a magnitude of 0.17 in the Unified Model compared to 0.27 in the ERA-40 dataset. Such a marked change is likely to be due to differences in the cloud and boundary-layer schemes used in the two models. To a lesser extent, impacts of the radiation field on other meteorological fields could be feeding back into the radiation field in this study – all meteorological fields from ERA-40 were prescribed in the study of Shonk and Hogan (2010).

We also include the global mean CRFs extracted from four months of data from the Earth Radiation Budget Experiment (ERBE; Ramanathan et al, 1989). These values are annual and global means, taken from April, July and October 1985, and January 1986; a period within our model runs. Again, we see differences between the observed radiation budget and the modelled radiation budget. In the short-wave, we find the ERBE global mean CRF to be similar to the ERA-40 mean value (-48.05 W m^{-2} compared with -49.72); in the long-wave, the ERBE CRF is more similar to the mean value from this study (30.98 W m^{-2} compared with 21.79 W m^{-2}). It is again likely that these differences are attributable to differences in cloud occurrence between the models and the observed clouds in ERBE.

A comparison of the horizontal and vertical shifts in short-wave and long-wave CRF show some large differences (most notably that the horizontal short-wave shift of Shonk and Hogan, 2010, is nearly twice the size of that of this study). However, it is seen in table 1 that, when expressed as percentages of the PPm CRFs, the shifts in each experiment are more similar. This suggests that the horizontal and vertical shifts in CRF are relative to the size of the CRF in a given model. The large differences in the net CRF shifts are due to the partial cancellation between the short-wave and long-wave CRFs, implying that small changes in short-wave and long-wave CRFs can give rise to a much larger net difference. The size of the shifts in net CRF are therefore very sensitive to the accuracy of the cloud distribution in the model.

The radiative behaviour of twenty general circulation models (GCMs) was compared by Bender et al (2006). They calculated monthly means of short-wave albedo from each of the GCMs over months from February 1985 to May 1989 (again, a period within our climate runs). The short-wave albedo that we calculate from our results from the Unified Model is 0.295, which compares well with the albedos reported by Bender et al (2006) for the HadGEM1 (0.296) and HadCM3 (0.295) configurations. The value from the

Table 2 Global mean shifts in two-metre temperature for this study, averaged over land points only (left columns) and over land points poleward of 45° in the winter hemisphere (right columns).

	All land points		*Winter land points > 45°*	
	DJF temp / °C	JJA temp / °C	DJF temp / °C	JJA temp / °C
Horizontal	−0.207	−0.062	−0.423	−0.111
Vertical	0.185	0.075	0.347	0.144
Total	−0.022	0.013	−0.076	0.033

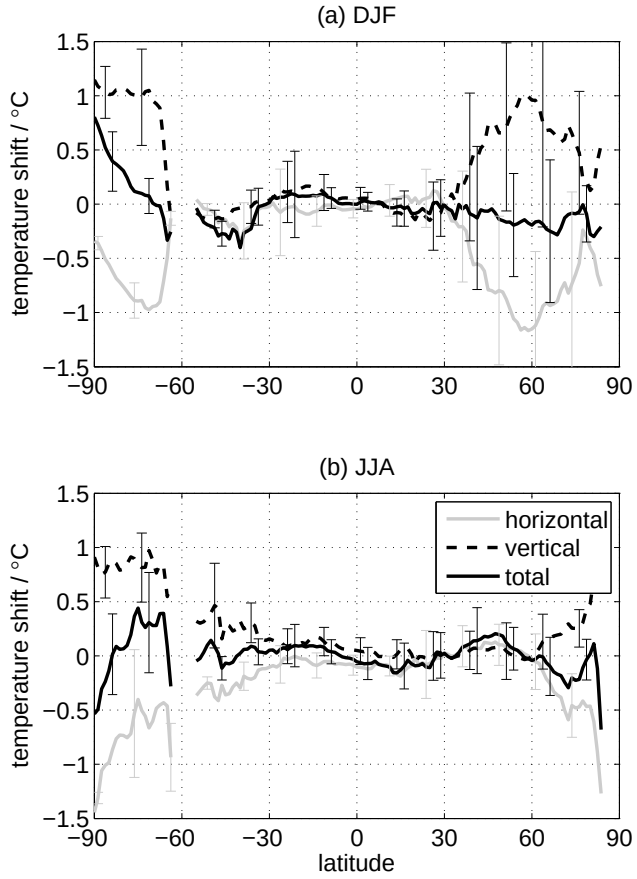

Fig. 8 Zonally averaged shifts in two-metre temperature, taken over land points only, as a function of latitude. Averages over all twenty years from (a) December, January and February and (b) June, July and August are shown, with error bars indicating the standard deviation at each latitude.

ERA-40 data is also within the range of albedos they found, at 0.311. Our horizontal and vertical shifts in short-wave albedo turn out to be −0.009 and 0.006 respectively. The standard deviation in mean monthly mean albedos across the models compared by Bender et al (2006) is 0.007. This implies that our horizontal and vertical shifts are of comparable size to the spread between their model albedos.

3.2 Shifts in two-metre temperature

Table 2 shows the global-mean shifts in two-metre temperature, averaged over land grid points only (both over all land surfaces, and land surfaces poleward of 45° in the winter hemisphere only). The distributions of global shifts in northern winter (December, January and February) and northern summer (June, July and August) are shown in figures 5 and 6 respectively, and zonal averages (again, over land points only) are shown in figure 8. As there is no influence of the atmosphere on sea-surface temperature, the temperature shifts over the ocean are near zero. For this reason, ocean points are excluded from zonal and global means. The seasonal averages are calculated over all twenty years, but only for the appropriate months. As shifts in temperature are not directly caused by the changes in cloud approximation, we perform a significance test to discover whether the shifts are greater in size than the natural variability. Areas of statistical significance are identified by comparing the temperature shifts with the natural variability of the temperature on a point-by-point basis. Significance was determined if the difference between the shift and the 20-year mean temperature exceeded a threshold that was related to the standard deviation of the temperature at that point over the 20 years. The black contour in figures 5 and 6 enclose regions where the shifts are statistically significant at 95%.

The most striking feature on these plots is the temperature change seen over land surfaces at high latitudes. The most notable shifts are in the winter hemisphere, with the introduction of cloud inhomogeneity leading to local coolings of up to 3°C and the improvement of cloud overlap causing warmings of similar magnitude. We see that the areas of largest shift are indeed within the significance contours. A simple mechanism for these temperature changes is presented in figure 7. In the winter poles, there is little solar insolation, so heating and cooling is mostly driven by long-wave interactions. An increase in cloud cover brought about by a change to the cloud overlap assumption, as shown in the left panel of figure 7, will therefore result in more radiation being emitted to the surface, causing a local warming (a positive temperature shift). The introduction of cloud inhomogeneity, as shown in the right panel, will act to reduce the plane-parallel biases not only in short-wave albedo, but also long-wave emissivity. This results in an inhomogeneous cloud of the same cloud cover and mean optical depth emitting less radiation to the surface causing a local cooling (a negative temperature shift). Examination of the shifts in CRF at the surface (not shown) supports this.

Dynamical feedbacks may also have enhanced the surface cooling over land at high latitudes. Specifically, enhanced radiative cooling of the air near the surface leads to a strengthening of the winter continental anticyclones via the mechanism proposed by Wexler (1937). This is confirmed

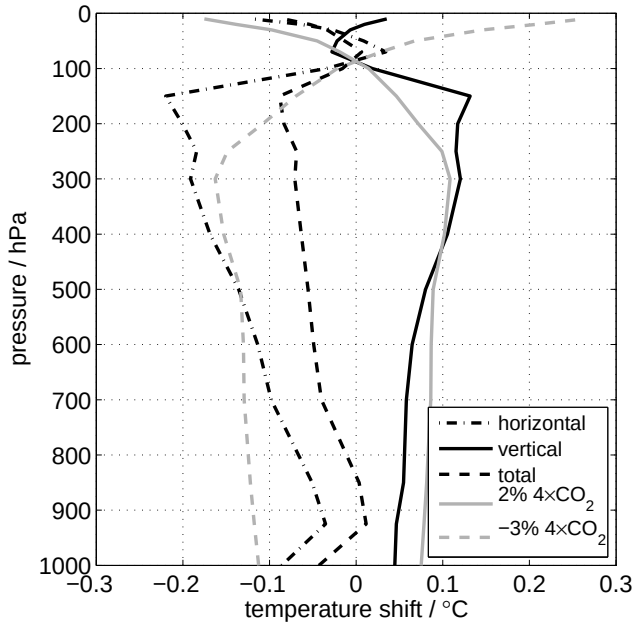

Fig. 11 Profiles of shifts in temperature, averaged over the twenty years and all gridpoints (both land and sea). The solid grey line indicates a profile of 2% of the temperature shift caused by a quadrupling of carbon dioxide applied to the HadGEM2 configuration of the Unified Model, based on results from CMIP5. The dashed grey line indicates a profile of -3% of the same shift.

by an increase of around 2 hPa in the DJF surface pressure in these regions when horizontal cloud inhomogeneity is introduced, as well as the associated increase in upper-troposphere convergence and lower-troposphere divergence. Higher pressure can then inhibit the incursion of low pressure systems, which would otherwise bring warmer air into the continental interior.

As a global mean, we see non-negligible shifts of order 0.05°C to 0.2°C over land (up to nearly 0.3°C over land north of 45° in northern winter). Again, as for the CRFs in the previous subsection, we see that there is cancellation between the horizontal and vertical shifts, with a small residual cooling for both seasons. Furthermore, the pattern of the total shifts in two-metre temperature in figures 5 and 6 shows neither a strong cooling or warming in the winter poles, but a residual of the two that varies in sign. This could be a further effect of the similarity in signs of the horizontal and vertical shifts in CRF.

3.3 Shifts in tropospheric temperature

We now turn our attention to the rest of the troposphere. Figure 9 shows the mean shifts in zonally averaged temperature, averaged over the full twenty years (all seasons). Contours of significance at 95% have been included in the figure. It is seen that changes to the state of the atmosphere are not just confined to the surface and the top of the atmosphere: we see that the temperature shifts noted at the polar surfaces extend into the lower troposphere, with the horizontal and vertical shifts cooling and warming the area respectively by of order 1°C. In some locations, however, these shifts are not significant, although natural atmospheric temperature variability above the surface can be large over the winter poles.

Introducing horizontal inhomogeneity is also seen to have a large and significant effect on temperatures in the upper tropical troposphere, with a cooling of over 0.5°C located over the equator at 200 hPa. The improved representation of vertical overlap causes a smaller, but still significant, warming, with the result that the combined effect of the two parameterizations is a small residual cooling. The temperature shifts are plotted as globally averaged profiles, in figure 11. The horizontal and vertical shifts (black lines) both show increased temperature shifts both at the upper troposphere and near the surface.

Figure 11 also contains temperature change profiles calculated using the HadGEM2 configuration of the Unified Model (Martin et al, 2011) as part of the CMIP5 project. An instantaneous quadrupling of carbon dioxide concentrations is applied, and the model run over a period of more than 100 years. This uses the same grid as our simulations, with the only difference being the presence of a coupling between the atmosphere and ocean. The plot shows the temperature change profile, averaged over all points globally and the final 15 years of the run, but scaled down by a factor of 50 (therefore representing 2% of the temperature shift; grey solid line). This line has been included to give an idea of the size of the vertical shift with respect to a standard climate response experiment. We also show a line representing -3% of the temperature shift to compare with the horizontal shift (dashed line). While the shapes of the lines are not perfect matches, we see that shifts are of comparable order of magnitude.

3.4 Shifts in cloud fraction

Temperature is not the only field that is affected by our improvements to the cloud structure representation. Figure 10 shows the shifts in zonally averaged cloud fraction, using exactly the same averaging as described for figure 9. Here, we see significant increases in cloud fraction in the upper tropical troposphere when cloud inhomogeneity is included, and reductions in cloud fraction in the same location when vertical overlap representation is improved. The largest changes in cloud fraction tend to be in the same locations as the largest temperature shifts. The simplest mechanism for this is that cooling the air at constant specific humidity will lead to a higher probability of condensation. The increase in tropical upper tropospheric cirrus in figure 10a could also be

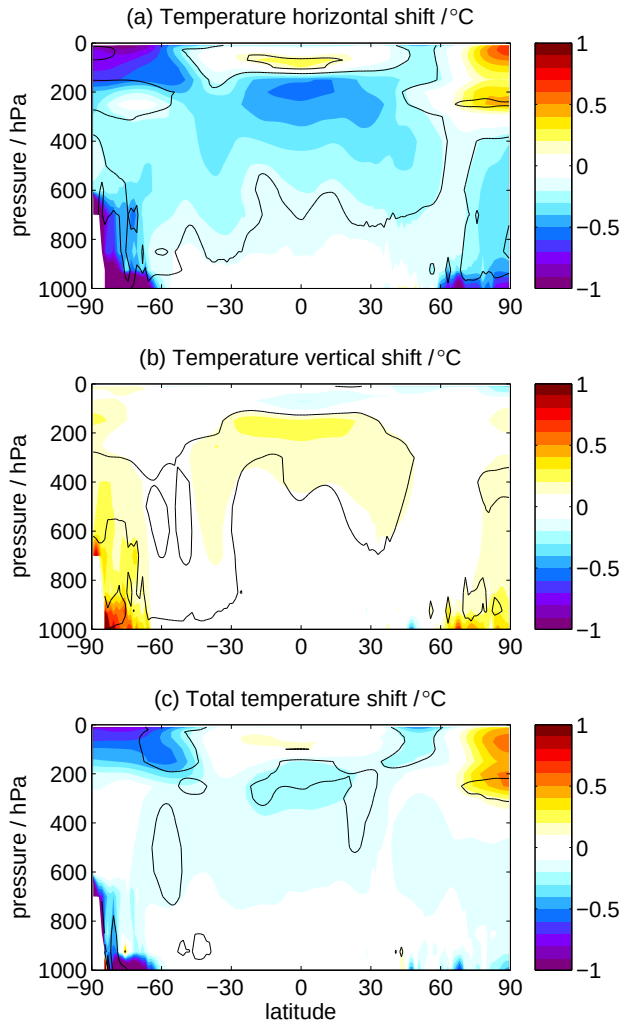

Fig. 9 Global distribution of shifts in zonally averaged temperature, averaged over the twenty years of the climate run: (a) horizontal shift, TCm minus PPm; (b) vertical shift, TCe minus TCm; and (c) total shift, TCe minus PPm are shown. The black line is a contour of significance at 95%.

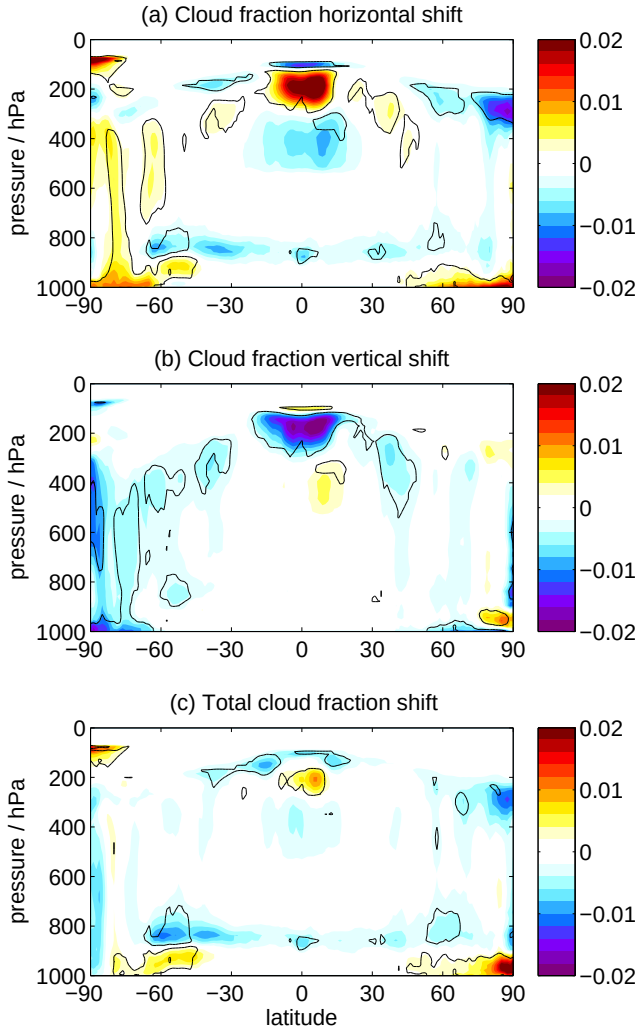

Fig. 10 Global distribution of shifts in zonally averaged cloud fraction, averaged the twenty years of the climate run: (a) horizontal shift, TCm minus PPm; (b) vertical shift, TCe minus TCm; and (c) total shift, TCe minus PPm are shown. The black line is a contour of significance at 95%.

caused by an increase in convective activity associated with a destabilization of the atmospheric profile.

In the polar regions we see an increase in near-surface cloud when inhomogeneity is accounted for. This cloud exists in the bottom few layers of the atmosphere, so could be a model version of radiative fog. The cooling of the surface by the processes described previously has been shown to cool the lower part of the atmosphere, so it is possible that more cloud will form in these lowest few layers. Figure 10a also reveals a decrease in boundary-layer cloud occurrence (between 800 and 900 hPa) when cloud inhomogeneity is accounted for, although the signal is only marginally significant. A possible hypothesis for this behaviour is that horizontally inhomogeneous clouds are less emissive in the long-wave, leading to weaker radiative cooling at cloud top, a weaker cloud-top inversion, greater entrainment of dry air into the boundary layer and a reduction in cloud amount. However, unlike the cloud changes in the tropical upper troposphere and the polar surface layer, the change to boundary-layer clouds appears not to be associated with a local change in temperature in figure 9a.

The chain of causality considered so far is that a change in cloud treatment in the radiation scheme (which does not affect cloud fraction) induces a change to the temperature field both of the atmosphere and the surface. This in turn affects the cloud fraction. Thus we have the possibility of *cloud radiative feedbacks* in that the changed clouds can then further modify the temperature field. These might be expected to be somewhat similar to those that act under carbon-dioxide-induced climate change (Stephens, 2005), although differences may arise on account of the fact that the original forcing is now not a carbon dioxide increase

but a change to the way the clouds themselves interact with radiation. As an example, the increase in tropical upper tropospheric cloud fraction in figure 10a is a response to a reduction in cloud emissivity and albedo associated with the introduction of cloud horizontal inhomogeneity. This therefore constitutes a negative feedback. As with all feedbacks, it is not large enough to fully counter the original forcing.

4 Conclusions

The need for cloud representation in climate models to be as realistic as possible is unquestionable. In this study, we performed twenty-year-long current climate simulations using improved representations of horizontal cloud inhomogeneity and vertical cloud overlap, both separately and in combination. The changes to the cloud representation were implemented solely within the radiation code. The control run used the standard plane-parallel clouds with maximum-random overlap; a second run introduced inhomogeneity using the "Tripleclouds" scheme; a third run combined this with "exponential-random" overlap. This approach allowed us to investigate the effects of the two parameterizations both separately and in combination.

Changing the cloud representation within the radiation code had significant effects, not just on radiation budget, but also other quantities. In terms of top-of-atmosphere cloud radiative forcing (CRF), we found that the change caused by introduction of inhomogeneity (the "horizontal shift") was of opposite sign to the change caused by the improvement of vertical overlap (the "vertical shift"). While the global-mean net CRF shifts were small (less than 1 W m^{-2} in magnitude), shifts of up to 10 W m^{-2} were found in locations where marine stratocumulus is dominant. We also found marked changes in two-metre temperature over land near the winter poles, with a cooling of up to 3°C imposed by the introduction of horizontal cloud structure and a warming of similar magnitude generated by improving vertical overlap. These temperature shifts were found to occur not only at the surface, but also up into the troposphere. The largest values of temperature shift were found in the upper tropical troposphere, and these were also found to affect the cloud distribution. Averaged globally, the magnitudes of the vertical and horizontal shifts were similar to about 2% of the temperature shifts caused by a quadrupling of atmospheric carbon dioxide.

In comparison to the shifts in radiation budget identified in ERA-40 reanalysis data by Shonk and Hogan (2010), it is seen that the magnitudes of the horizontal and vertical shifts are far more similar in this study, leading to a much smaller net shift. While some of this could, in principle, be due to the fact that clouds in this study are allowed to change and therefore feedback on the radiation, we attribute most of the difference with Shonk and Hogan (2010) to very different cloud radiative forcings (CRF) in the control climate of the two models. Specifically, the global-mean short-wave CRF is 37% larger in the ECMWF than the Unified Model (see Table 1), while in the net is a factor of two larger. Despite the differences between the two models, both provide mean short-wave albedos that lie in the range of values set out by Bender et al (2006). In fact, the size of the shifts in albedo due to the addition of cloud structure are comparable to the size of the uncertainty in albedo across all of the models they compared. Moreover, the difference of 18.2 W m^{-2} between the global-mean net CRFs in the two models is less than the 32 W m^{-2} range found in 19 atmospheric general circulation models by Potter and Cess (2004).

Unfortunately, our ability in Shonk and Hogan (2010) and in the present paper to quantify the net effect of cloud structure globally is dependent on the nature of the short-wave and long-wave cloud–radiation interactions in the model used. Therefore, the large degree of cancellation found between horizontal and vertical shifts in this study may well be less strong in other climate models. Nonetheless, we reiterate the point made by Shonk and Hogan (2010) that the fact there is some degree of cancellation indicates that it is important to address the representation of horizontal inhomogeneity and vertical overlap simultaneously; addressing one but not the other is likely to lead to a worsening of the way clouds interact with radiation.

A latitude-dependent parametrisation in a climate model has the potential to lead to artificial results that are constrained by latitude. In theory, exponential-random overlap could be improved by connecting the decorrelation height to cloud type instead of latitude so that any changes to cloud distribution also affect the nature of the cloud overlap in a given location. Alternatively, a global value of decorrelation height could be applied, such as the 2 km proposed by Barker (2008). It was shown by Shonk and Hogan (2010) that, while the radiation budget is very different when maximum-random overlap is replaced by exponential-random overlap, it is fairly insensitive to the exact choice of decorrelation height. Nevertheless, a latitude-dependent parametrisation based on that of Shonk et al (2010) has recently been implemented in the ECMWF model (JJ Morcrette, personal communication).

A further aspect of this work that could be refined in future is our use of an atmosphere-only model with prescribed sea-surface temperatures. A better estimate of the full effects of cloud structure on climate would require a similar investigation with a fully coupled model that allowed both the ocean and the sea ice to vary in response to the changes to the atmosphere. This would allow us to more fully investigate the effects of cloud structure on atmospheric state over the course of a climate simulation.

Acknowledgements We thank the following people at the Met Office for their help, support and advice: Jon Petch, Cyril Morcrette, Dan Copsey, Jonathan Wilkinson, Peter Hill, Terry Davies, David Hassell, Khalid Mahmood and Andy Macallan. We also thank Keith Shine for some very useful discussions, Loïs Steenman-Clark for advice on getting started with the Unified Model, and Ed Hawkins for help with CMIP5 data. This work was supported by NERC grants NE/F011261/1 and NE/G016038/1.

References

Barker HW (2008) Overlap of fractional cloud for radiation calculations in GCMs: a global analysis using CloudSat and CALIPSO data. Journal of Geophysical Research 113:DOI: 10.1029/2007JD009,677

Barker HW, Stephens GL, Fu Q (1999) The sensitivity of domain-averaged solar fluxes to assumptions about cloud geometry. Quarterly Journal of the Royal Meteorological Society 125:2,127–2,152

Bender FA, Rodhe H, Charlson RJ, Ekman AML, Loeb N (2006) 22 views of the global albedo – comparison between 20 GCMs and two satellites. Tellus 58A:320–330

Brown PRA, Francis PN (1995) Improved measurements of the ice water content in cirrus using a total-water probe. Journal of Atmospheric and Oceanic Technology 12:410–414

Cahalan RF, Ridgway W, Wiscombe WJ, Bell TL, Snyder JB (1994) The albedo of fractal stratocumulus clouds. Journal of the Atmospheric Sciences 51:2,434–2,455

Carlin B, Fu Q, Lohmann U, Mace GG, Sassen K, Comstock JM (2002) High-cloud horizontal inhomogeneity and solar albedo bias. Journal of Climate 15:2,321–2,339

Edwards JM, Slingo A (1996) Studies with a flexible new radiation code. Part I: choosing a configuration for a large-scale model. Quarterly Journal of the Royal Meteorological Society 122:689–719

Geleyn JF, Hollingsworth A (1979) An economical, analytical method for the computation of the interaction between scattering and line absorption of radiation. Contribution to Atmospheric Physics 52:1–16

Hogan RJ, Illingworth AJ (2000) Deriving cloud overlap statistics from radar. Quarterly Journal of the Royal Meteorological Society 126:2,903–2,909

Martin GM, Bellouin N, Collins WJ, Culverwell ID, Halloran PR, Hardiman SC, Hinton TJ, Jones CD, McDonald RE, McLaren AJ, O'Connor FM, Roberts MJ, Rodriguez JM, Woodward S, Best MJ, and Co-authors (2011) The HadGEM2 family of Met Office Unified Model climate configurations. Geoscientific Model Development Discussions 4:765–841

Oreopoulos L, Barker HW (1999) Accounting for subgridscale cloud variability in a multi-layer 1D solar radiative transfer algorithm. Quarterly Journal of the Royal Meteorological Society 125:301–330

Pincus R, Barker HW, Morcrette J (2003) A fast, flexible, approximate technique for computing radiative transfer in inhomogeneous cloud fields. Journal of Geophysical Research 108:DOI: 10.1029/2002JD003,322

Pomroy HR, Illingworth AJ (2000) Ice cloud inhomogeneity: quantifying bias in emissivity from radar observations. Geophysical Research Letters 27:2,101–2,104

Potter GL, Cess RD (2004) Testing the impact of clouds on the radiation budgets of 19 atmospheric general circulation models. Journal of Geophysical Research 109:DOI: 10.1029/2003JD004,018

Ramanathan V, Cess RD, Harrison EF, Minnis P, Barkstrom BR, Ahmad E, Hartmann DL (1989) Cloud radiative forcing and climate: results from the Earth Radiation Budget Experiment. Science 243:57–63

Randall DA, Wood RA, Bony S, Colman R, Fichefet T, Fyfe J, Kattsov V, Pitman A, Shukla J, Srinivasan J, Stouffer RJ, Sumi A, Taylor KE (2007) Climate Change 2007: the Physical Science Basis. Contribution of Working Group I to the Fourth Assessment Report of the Intergovernmental Panel on Climate Change, Cambridge University Press, chap 8: "Climate models and their evaluation"

Shonk JKP, Hogan RJ (2008) Tripleclouds: an efficient method for representing cloud inhomogeneity in 1D radiation schemes by using three regions at each height. Journal of Climate 21:2,352–2,370

Shonk JKP, Hogan RJ (2010) Effect of improving representation of horizontal and vertical cloud structure on the earth's global radiation budget. Part II: the global effects. Quarterly Journal of the Royal Meteorological Society 136:1,205–1,215

Shonk JKP, Hogan RJ, Mace GG, Edwards JM (2010) Effect of improving representation of horizontal and vertical cloud structure on the earth's global radiation budget. Part I: review and parametrisation. Quarterly Journal of the Royal Meteorological Society 136:1,191–1,204

Slingo A (1990) Sensitivity of the Earth's radiation budget to changes in low clouds. Nature 343:49–51

Stephens GL (2005) Cloud feedbacks in the climate system: a critical review. Journal of Climate 18:237–273

Wexler H (1937) Formation of polar anticyclones. Monthly Weather Review 65:229–236